Robot-Assisted Bone Cement Injection

Nicole Neumann, Laurence Meylheuc, Laurent Barbé, Julien Garnon, Guillaume Koch, Afshin Gangi, Bernard Bayle

Robot-Assisted Bone Cement Injection

N. Neumann, L. Meylheuc, L. Barbé, J. Garnon, G. Koch, A. Gangi and B. Bayle*

***Abstract*—In this article, assistance to bone cement injection is studied, with a focus on vertebroplasty, a procedure dedicated to the treatment of vertebral compression fractures. A robotic system that can remotely be operated at pressures up to 140 bar is presented. It improves cement polymerization control, combining a cold passive exchanger that slows down the cement curing in the syringe and an active exchanger that controls the injected cement temperature. The cement remote injection uses a rate control teleoperation strategy with force feedback to help monitoring the cement state. In addition to laboratory assessments, cadaver experiments were performed to illustrate the satisfactory operation of the whole system.**

***Index Terms*—Medical robotics, Percutaneous vertebroplasty.**

I. Introduction

The spine, made up of 33 bones, plays a major role in the posture and the locomotion. Each vertebra presents a solid ventral part, called vertebral body, which consists of cancellous bone, surrounded by a thin protective layer of hard cortical bone. The vertebral body is likely to collapse under significant compression efforts, resulting in a Vertebral Compression Fracture (VCF) that decreases the vertebral height and modifies the spine curvature, sometimes critically. The associated pain may worsen severely the quality of life and the functional abilities. These fractures often result from osteoporosis, which occurs predominantly in women [1] with nearly one in two women suffering from VCF after the menopause. Besides, as the population continues to age, osteoporotic VCF prevalence continues to rise. The treatment of VCF is often conservative, with bed rest and analgesics, even after several months of pain. In light of this growing public health problem, minimally invasive procedures have developed [2]. Known under the name of percutaneous cementoplasty, these image-guided interventions consist in injecting percutaneously synthetic bone cement into the vertebral body to stabilize the fractured vertebra, with an immediate and significant decrease of pain. The present study focuses on vertebroplasty, though the proposed method may apply to other cementoplasty procedures.

In spite of major advantages, vertebroplasty procedures also have major drawbacks. The first two drawbacks result from the polymer properties. When the procedure starts, the cement has to be sufficiently liquid to enable manual injection, thus increasing the risk of leakage outside the vertebral body. Cement leakage, which occurs in up to 20% of vertebroplasty procedures, is symptomatic in 1.6% of the procedures [3] with complications that range from lumbar pain to pulmonary embolism. Therefore, a waiting phase of $1-3$ min is recommended by cement manufacturers to allow cement viscosity increase after mixing of the cement components (powder and liquid). Another drawback comes from cement fast hardening at the end of the application phase that limits the injection time to $10-20$ min, depending on the cement and the room temperature. The intervention has to be ended and the needles removed before this abrupt hardening. The last main drawback of vertebroplasty comes from the use of X-ray imaging to supervise the spreading of the cement inside the vertebral body. This leads to the continuous exposure of the practitioner [4], only partially limited by uncomfortable lead clothes.

Vertebroplasty includes CT-guided trocars positioning followed by the fluoscopy-controlled cement injection. Positioning and inserting the trocars is well mastered by the practitioners who, in addition, do not suffer from over-exposition to X-rays during trocars insertion. As a result, the assistance to vertebroplasty should first focus on the cement injection. The objective of this article is to introduce a novel device specifically designed to facilitate both cement injection control and staff protection. Acrylic cement assisted injection has been considered by only a few studies in the past. In their pioneering work Loeffel *et al.* [5] present a system that performs remote vertebroplasty with force feedback, but without any management of cement viscosity. The StabiliT© system from Merit Medical [6] offers an interesting solution to polymerize bone cement *in situ* using radiofrequencies but the practitioner does not receive any feedback. These two strategies partly inspired the present work whose contributions are the development of a new method to perform both teleoperation with haptic feedback and viscosity management. The proposed system and methods allow using classical cement and estimate its viscosity, which is a key factor in leakage management that is fully subjective with current devices.

The study is organized as follows. Section II surveys the main characteristics of bone cement injection from a user's perspective. Medical constraints and properties related to bone cement polymerization are particularly emphasized, to list the specifications for vertebroplasty assistance. These specifications are then exploited in section III, which focuses on the design of a novel and dedicated device. The system operation is developed in section IV, including temperature control technology, remote operation and viscosity management. Experiments in near clinical conditions are then provided in section V in order to illustrate the performance of the system. Finally, section VI sums up the main contributions and opens perspectives for future research.

Manuscript received *XX*, 2021.

N. Neumann, L. Barbé, and B. Bayle* (corresponding author) are with ICube Laboratory, UMR CNRS 7357, Strasbourg, France and University of Strasbourg (e-mail: bernard.bayle@unistra.fr). L. Meylheuc is with ICube Laboratory, UMR CNRS 7357, Strasbourg, France and INSA Strasbourg. G. Koch is with the Anatomy Department and the Interventional Imaging Department of the University Hospitals of Strasbourg. J. Garnon and A. Gangi are with ICube Laboratory and Interventional Imaging Department of the University Hospitals of Strasbourg.

II. Medical motivation and specifications

A. Percutaneous vertebroplasty procedure

During a vertebroplasty, the patient is, most of the time, placed in prone position on the table of the imaging device. Patients receive local anesthesia with mild sedation and analgesia, except for some long or complex interventions. Commonly, two types of peroperative imaging are combined: Computed Tomography (CT) for its high spatial resolution and X-ray fluoroscopy for continuous imaging [7]. Prior to the intervention, a planning step determines the insertion line of the trocar, which is the medical tool used to reach the vertebral body. The trocar, measuring from 10 to 13G in diameter, is made up of a hollow tube, called cannula, and a solid central stylet. For thoracic and lumbar levels, it is hammered inside the vertebra following a transpedicular approach [8] (see Figure 2(a)), using CT imaging to precisely guide the tool amid the adjacent vascular, neurological and visceral structures [9]. When several vertebrae are planned to be cemented, all the required trocars are first inserted, before any injection. During the positioning of the trocars, radiation exposure is relatively low since the medical staff can step out of the X-ray area during the acquisition of images. Then, the injected material can be prepared.

Among all orthopedic cements, acrylic bone cements, based on Poly(Methyl MethAcrylate) (PMMA), are the most employed material in vertebroplasty because of their high mechanical strength. PMMA is obtained by mixing two components, a polymeric powder and a monomeric liquid. Among others, the powder incorporates an initiator to encourage the polymerization at room temperature, and a radiopacifier to make the cement visible in fluoroscopic images. The mixing process ends when a homogeneous blend is acquired, the powder being then fully dissolved in the liquid and the bone cement relatively liquid. The mixture is introduced in the chosen injection device. The central needle stylet being removed from the inserted trocar, the injection system can be plugged to the cannula either directly or via a connecting hose that is preferably short, in order to limit cement loss in the pipes and to have a better control of the injection.

The injection can then start. During the injection, continuous fluoroscopy allows monitoring the bone cement diffusion inside the vertebral body. Radiation exposure is then high [10], as the practitioner stays very close to the imaging device because of the short length of the connecting hose. Approximately 30% to 50% of the vertebral body is filled with bone cement, which is equivalent to $3-4$ mL for a thoracic vertebra and $5-7$ mL for a lumbar vertebra. The injection has to be completed and the needle has to be removed before the bone cement hardens totally. This emphasizes that the practitioner must have a very good knowledge and control of the injected bone cement. This is all the more challenging that manufacturers do not provide any viscosity quantification, useful information being limited to handling properties such as in Figure 1 for Osteopal® V bone cement from Heraeus. However, the polymerization process of bone cement is exothermic and the temperature room highly influences the reaction's time.

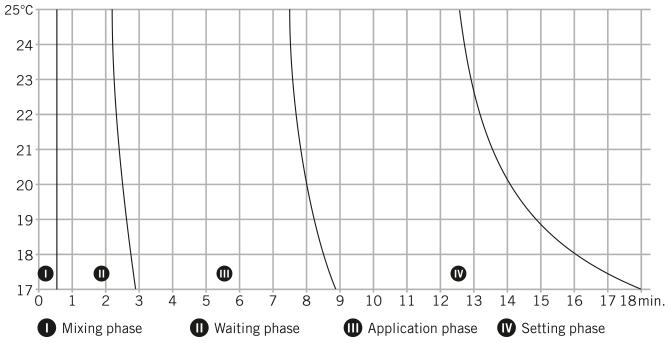

Figure 1. Temperature-dependent handling properties for Osteopal® V bone cement (courtesy Heraeus Medical).

The intervention lasts between 30 minutes and 2 hours, depending on the number of vertebrae to be healed but also on the physician's experience. To validate the good and uniform filling of the vertebral body, a final X-ray imaging step is performed, as in Figure 2(b) where images were acquired at the Interventional Imaging Department of University Hospitals of Strasbourg (HUS) during a vertebroplasty procedure performed by Dr. J. Garnon.[1]

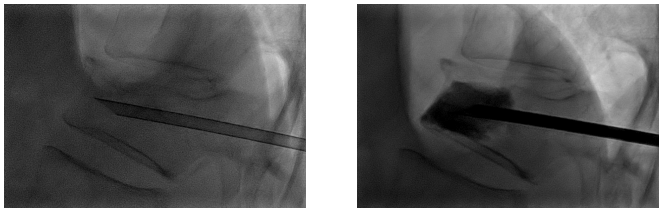

(a) (b)

Figure 2. Left lateral fluoroscopic image of a lumbar vertebroplasty: (a) after the trocar positioning; (b) after the cement injection.

B. Specifications for vertebroplasty assistance

1) Operation: A system dedicated to vertebroplasty assistance should consider the radiation protection of the medical staff, which means that the control of the injection device should be performed remotely. It should allow bone cement injections at very slow flow rates, which is tiresome for the operator, and, above all, not accurate.

2) Cement flow: Statistics based on interventions made at HUS allowed measuring a mean cement flow rate of $Q_{v_{\text{mean}}} \simeq 35\ \text{mm}^3 \cdot \text{s}^{-1}$. An injection system should also prevent cement from continuing to flow when the practitioner halts the injection to check the cement diffusion or when the injection is finished. This adverse event can lead to leakages [5], [11].

3) Bone cement viscosity range: To the best of our knowledge, the only work evoking viscosity at which the injection should be started or ended is proposed by Giannitsios *et*

[1]The patient gave informed consent for the procedure and the publication of anonymized data. Data collection and experiments presented in this article were approved by the ethical committee of HUS. The data collection and reuse were made in accordance with the Data Protection Act stating that all the data concerning the patient are treated with the strictest confidentiality.

al. [12], who suggest to use $\eta_{\min} = 350\,\text{Pa}\cdot\text{s}$. This value seems reasonable according to our experiments, but it should be noted that it remains highly subjective. Maximum admissible viscosity, a key specification related to the maximum force applied to the injection device piston, has been studied from experiments with a rotational rheometer, using several acrylic bone cements [13]. PMMA-based cements show a complex behavior since they present shear-thinning, thermo-dependent and time-dependent viscosity. For design purpose, the worst case was considered. According to the cement handling properties of Figure 1, the working phase should never last more than 9 min, which corresponds to $\eta_{\max} = 1689\,\text{Pa}\cdot\text{s}$ on the viscosity evolution curve of Osteopal® V, given in Figure 3. This experiment has been carried out for $\dot{\gamma} = 0.2\times 2\pi\ \text{s}^{-1}$, the average shear-rate in the needle, at ambient temperature, on a rotational rheometer HAAKE™ MARS™ from ThermoFisher Scientific with 10 mm radius parallel-plates and a gap size of 1 mm. With a safety margin, the maximum viscosity value $\eta_{\max} = 2000\,\text{Pa}\cdot\text{s}$ was finally selected.

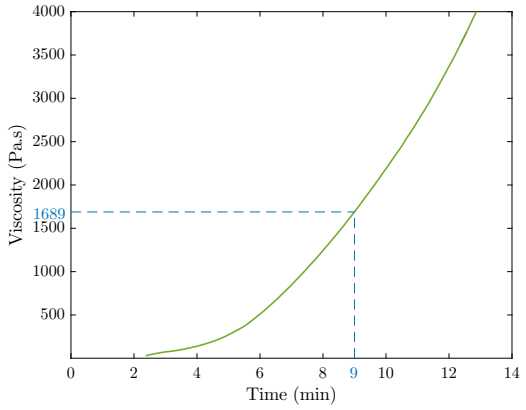

Figure 3. Viscosity evolution of Osteopal® V cement (Heraeus) acquired with a rotational rheometer with $\dot{\gamma} = 0.2\times 2\pi\ \text{s}^{-1}$ and at ambient temperature where time zero represents the beginning of the mixing phase.

4) Viscosity management: The evolution of bone cement viscosity is strongly influenced by the procedure conditions, particularly by the temperature [13], [14]. Cool down bone cement results in low cement viscosity and a longer setting phase. So, it is common to store the cement kit inside a refrigerator near the operating room until the immediate start of the cement mixing. As previously mentioned, the polymerization reaction that undergoes the bone cement is highly exothermic (up to $80-100\,^{\circ}\text{C}$), as exposed in Figure 4 for three different commercial bone cements. These temperature measurements were performed with a thermocouple inserted in the middle of a $60\,\text{mm}\times 6\,\text{mm}$ polymerizing cement mass, as defined by the ISO 5833:2002 [15].

Extracting thermal power from the bone cement will slow down the polymerization and, thus, increase the working phase. According to Figure 4, this thermal power denoted as P_t, should at least prevent a temperature increase of $80\,^{\circ}\text{C}$. For a flow rate Q_v, this condition is written $P_t > 80\rho c Q_v$, where ρ and c represent the density and the specific heat capacity of the considered cement, respectively. With the numerical values

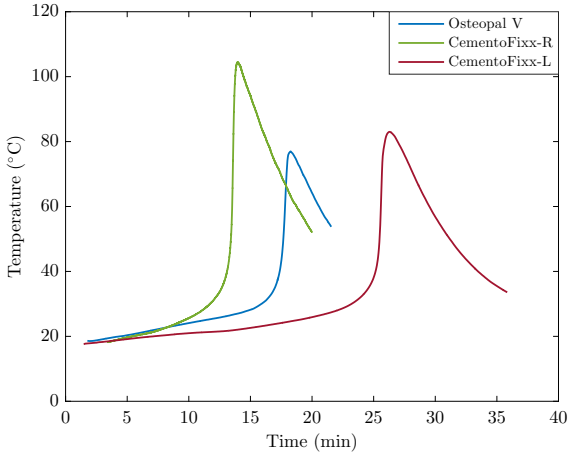

Figure 4. Temperature measurements during polymerization for Osteopal® V cement from Heraeus, CementoFixx-R and CementoFixx-L from Optimed, where time zero represents the beginning of the mixing phase.

from [16], it follows that $P_t > 5\,\text{W}$. This value can of course be adapted to increase the thermal effect or to improve the performance of the exchanger.

III. Design

A. Injection devices

Most commercial systems for bone cement injection are manually-operated. They include a syringe whose piston is pushed either by hand, as the Vertecem® II system from DePuy Synthes [17], or via a force amplification mechanism, as the Precision Cement Delivery System® from Stryker [18] or the Optimed Cemento MP® [19] that both use a screw-nut system. Some manufacturers propose injection devices that allow increasing the distance between the practitioner and the X-rays source. The Confidence Spinal Cement System® from DePuy Synthes [17] and the Osseoflex® device from Merit Medical [6] perform such remote injections with hydraulic transmission lines ($0.5-1.5\,\text{m}$ long). However, such transmissions add uncertainty and latency, resulting in a lack of control for the practitioner. Typically, it is impossible to stop the injection fast, resulting in an increased risk of leakage.

Only a few systems offer a solution to cope with the complications and drawbacks stated in section I. The StabiliT® from Merit Medical [6] is a unilateral teleoperation device. It uses a special low viscosity cement whose curing is handled by applying radiofrequency waves before its injection into the vertebral body, which highly limits the risk of leakage. The two main limitations of this system comes from i) its high cost, $1000-3000€$ per treated vertebra; ii) its on/off operation, which results in the loss of force feedback during the injection. Paradoxically, the use of force feedback has not extensively been studied, Loeffel et al. [5], [20] providing the only reference in the field. Their system consists of an injection device with advanced supervision functions, able to deliver cement at high viscosity. Injection pressures up to 50 bar are obtained with the system that can be operated at a distance. The shape of the interface design recalls that of a

syringe, and it can provide passive force feedback provided by a magneto-rheological fluid. Other interesting functionalities, as the estimation of the injected fluid viscosity, and a flow-stop mechanism are proposed. Though the system was only validated in a laboratory configuration, this pioneer work [5] opens up several research avenues, such as the online identification of viscosity, the user interface operation, or the presence of flow obstructions. These are some of the concerns that are developed in the following.

B. Teleoperated injection system

1) Disposable elements: Disposable items gather syringes containing the bone cement to be injected and trocars in order to reach the fractured vertebral body. At least 10 mL-syringes must be selected, without exceeding a volume of 15 mL, in order to remain consistent with most commercial bone cement kits. A Luer Lock connector is required to ensure the connection between the syringe and the cannula at high pressures and a centered outlet is preferred so that the flow stays axisymmetric. The chosen 10 mL-syringes with 1.9 mm thick Premium® polymer walls from Ardes [21] meet the application requirements: they can be disassembled and resist to high temperatures. Their inner radius is $R_s = 7.1$ mm. According to usual vertebroplasty procedures where trocars ranging from 10 to 13 G are employed, 11 G cannulas with an inner radius of 1.25 mm were used for all the experiments.

2) Bone cement injection system: Assuming a Poiseuille flow, the principle of mass conservation, coupled to the resolution of the Navier-Stokes equation, leads to a relationship between the flow rate Q_v and the pressure drop ΔP along a conduit of length L_c and of radius R_c [22]:

$$\Delta P = \frac{8\eta L_c Q_v}{\pi R_c^4} \tag{1}$$

where η represents the viscosity of a Newtonian fluid. A maximum pressure drop $\Delta P_{\max} \simeq 140$ bar is then obtained for $\eta = \eta_{\max} = 2000\ \mathrm{Pa \cdot s}$, $Q_v = Q_{v_{\mathrm{mean}}} = 35\ \mathrm{mm^3 \cdot s^{-1}}$, $L_c = L_{c_{\max}} = 20$ cm, based on recommendations from practitioners, and $R_c = 1.25$ mm. Then, given the radius of the selected syringes, the maximum force is $F_{\max} \simeq 2200$ N.

The designed injection device, represented in Figure 5, is based on a ball screw linear axis allowing the translation of the piston that pushes the bone cement with pressures up to 140 bar. The linear axis combines a linear guide and a ball

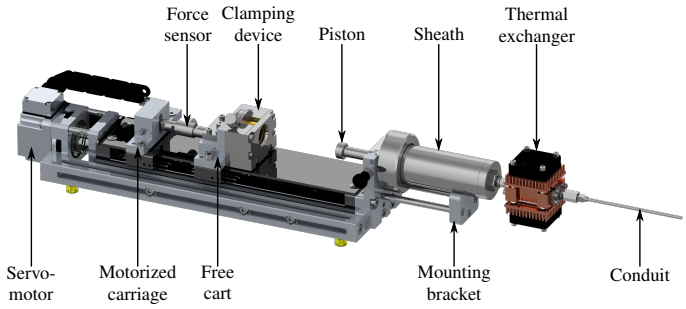

Figure 5. CAD view of the injection device.

screw from Misumi, with a 5 mm-pitch. The screw itself is motorized by a servo-motor FHA-8C from Harmonic Drive with an 1.5 N·m nominal torque. The device is equipped with two carriages, one directly mounted on the nut while the second one can move freely along the rail. A manual clamping device placed on the free cart allows gripping the syringe piston. Both carriages are coupled by a 2 kN uniaxial tension-compression force sensor from Scaime. The resolution is below 1 µm for the translation, and below 0.1 N for the force measurement. A mounting bracket allows to easily plug and remove the stainless steel sheath in which the syringe perfectly fits to resist high pressures. The sheath can be sterilized, which guarantees the asepsis of the system once the syringe filled with cement and the piston are in place. The overall dimension of the system is 54 cm×12 cm×10 cm. The system is placed on a cart near the patient, connected to the trocar through the conduit visible in Figure 5. Unlike in [5] , it has a small footprint in the operating scene, but, in this way, the patient's fragile vertebrae are not exposed to any extra load.

3) Haptic device: A device was designed to control remotely the injection and to render force feedback representing cement hardening to the practitioner, up to 19.9 N. It has been built around a cable-driven pulley-capstan transmission [23], illustrated in Figure 6. The workspace ranges from 0 (at rest) to 60 deg and the position is measured by the motor encoder, with a theoretical angular resolution lower than 0.01 deg at the user hand. An optional 100 N force sensor (Scaime), with a 0.02 N resolution allows assessing force feedback performance.

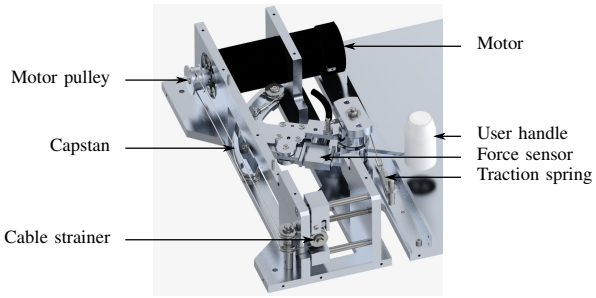

Figure 6. CAD view of the haptic interface.

C. Thermal exchangers

1) Principle: Viscosity management can be obtained by cement temperature control. Ideally, the thermal bone cement temperature control should be as close as possible to the treated vertebra, as for the StabiliT® system [6]. However, introducing an active thermal element inside the vertebral body comes at the expense of additional complexity and costs. Besides, the cement flowing upstream in the circuit is likely to form a stopper. So, the thermal exchanger should rather stand at the syringe level. However, the thermal diffusivity of acrylic bone cements is so small that temperature variations at the center of a typical 10 mL-syringe are very slow, and not adapted to the intervention duration. Following these observations, it is proposed to place two thermal exchangers along the cement flow: one at the syringe level to cool down the cement and another one at the output of the syringe where the small flow cross section area allows maximizing cement temperature control (see Figure 7).

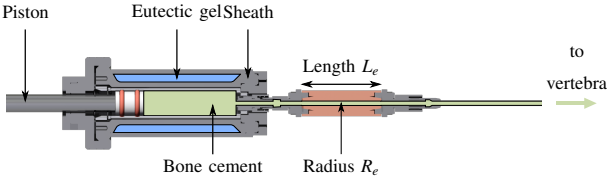

Figure 7. Cutout drawing of the bone cement flow showing the positioning of the passive cooling system to delay cement polymerization in the syringe, and the active thermal exchanger to control the flowing cement temperature.

2) Passive thermal exchanger: The passive cooling is carried out by filling cavities inside the sheath with Cryopak Phase 22 eutectic gel, indicated in blue in Figure 7. It was chosen for its phase change point at 22 °C that is appropriate for applications requiring temperatures between 10 °C and 40 °C. By leaving the empty sheath inside the refrigerator prior to the intervention, cement is then kept sufficiently cool to slow down the polymerization rate. For instance, for Osteopal® V cement, this leaves more than 30 min to inject the cement, which is about three times longer than usual.

3) Active thermal exchanger: The length L_e of the active thermal exchanger and the radius R_e of its inner conduit are selected to allow varying the temperature of the flowing cement within an acceptable time. In order to maintain the whole pressure drop in the portion between the syringe and the cannula, and to allow computing online the cement viscosity, there is no cross-section reduction downstream of the syringe exit. Therefore $R_e = R_c = 1.25$ mm, which is the radius of the selected 11 G cannula. Viscosity control limits possible occlusion issues within this small conduit. The transit time t_{transit} of the cement inside the thermal exchanger has to be longer than the $t_{5\%}$ settling time required for a cement particle, moving from the inlet of the thermal exchanger to its outlet, to reach a given temperature. As $Q_v t_{\text{transit}} = \pi R_e^2 L_e$, L_e can be obtained for $R_e = 1.25$ mm by solving numerically the heat equation for a cement cylinder of radius R_e flowing at $Q_v = Q_{v_{\text{mean}}}$. For an initial temperature $T_{\text{init}} = 40$ °C and an imposed temperature $T_{\text{imp}} = 10$ °C, $t_{5\%} = 6.5$ s, leading to the minimum length of the exchanger $L_{e_{\min}} = 45$ mm.

ThermoElectric Modules (TEMs) have been selected as they provide a flexible, lightweight and small size solution, with a fast response time. The components choice is made considering the theoretical thermal power of 5 W that has to be extracted, the TEM poor efficiency estimated to $30-50\%$ and the minimal length $L_{e_{\min}}$. The selected QC-63-1.4-8.5M TEMs from Quick-Cool perfectly fit the exchanger dimensions, and are voluntarily oversized in terms of power (maximal thermal power of 37 W), to allow fast temperature variations. The active thermal exchanger (see Figure 8) is composed of a central block made of copper, known for its high thermal conductivity, and two symmetric stacks associating a TEM, a heat sink and a fan. This configuration maximizes thermal efficiency by lowering the temperature difference between the hot and cold side of each TEM. The central block is crossed by a cylindrical channel through which the bone cement flows. A thermal insulation wrapping reduces exchanges with ambient air. Two Luer Lock connectors link each extremity of the channel, respectively to the syringe and the conduit. The whole exchanger has a size of 45 mm × 45 mm × 60 mm.

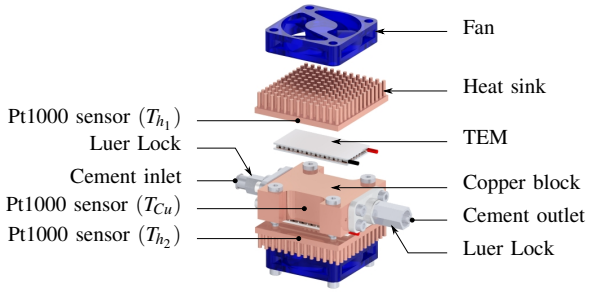

Figure 8. Exploded view of the active thermal exchanger.

4) Validation: Finite Element Method simulations were performed in order to validate the geometry of the thermal exchanger. The settling time was checked, as the heat transfer capability, especially the time delay necessary to equalize the difference between the copper temperature T_{Cu} and the bone cement one.

The bone cement rheological behavior was modeled by the power-law:

$$\eta(t) = K(t)\dot{\gamma}^{n-1} \tag{2}$$

where $\dot{\gamma}$ represents the shear rate and n, fixed at 0.2, the flow index. K, the flow consistency, was identified as the sum of two exponential functions [13] such that $K = a_K \exp(b_K t) + c_K \exp(d_K t)$ with $a_K = 3.078 \cdot 10^{-8}$ Pa·s^n, $b_K = 1.791 \cdot 10^{-2}$, $c_K = 429.6$ Pa·s^n and $d_K = 2.684 \cdot 10^{-3}$. The simulation considered that the cement enters at 40 °C in the exchanger and flows at $Q_v = Q_{v_{\text{mean}}} = 35$ mm$^3 \cdot$s^{-1} and that the cold side of the TEM is set at 10 °C. The temperature evolution at the outlet of the block and the settling time at the center of the stream were then identified. As expected, a slight delay of about 5 s is noticeable, which corresponds to the time required to reach the center of the cement flow. The simulation confirms the adequate dimensioning since the settling time is lower than the transit time of the cement in the pipeline.

IV. Control

A. Teleoperation

In bilateral telemanipulation, the operator handles the haptic interface while the remote device interacts with the environment. The objective is to provide the operator the best immersion in the remote scene while ensuring stability. Immersion is characterized by transparency, which classically reflects the matching between the impedance Z_{th} experienced by the operator and the environment impedance Z_e [24]. This criteria is applied to design more or less transparent teleoperation systems, resulting from a compromise with stability, analyzed by applying rules such as Llewellyn's absolute stability criterion [24]. In our case, the injection device is not backdrivable and the force applied to the cement is measured. As a result, the 2-channel force-position teleoperation architecture of Figure 9 is convenient. In this figure, the velocity V and force F signals of the human operator, the haptic interface, the injection device, and the environment correspond to the respective indexes h, m, s and e. F_h^* models the intention of

the operator, and it is assumed that external disturbances on the environment are negligible. In addition G_m and G_s respectively represent the haptic interface and injection device closed-loop transfer functions. As $F_e = C_1 G_s Z_e V_h$ and $V_h = G_m(F_h - F_e C_2)$, the transmitted impedance is $Z_{th} = G_m^{-1} + C_1 C_2 G_s Z_e$ and satisfactory transparency is then obtained by tuning carefully the injection device local loops so that $G_s \simeq 1$ and by selecting $C_2 = C_1^{-1}$. This leads to $Z_{th} = G_m^{-1} + Z_e$ where the impedance of the closed-loop control master G_m^{-1} is minimized to meet the transparency requirement.

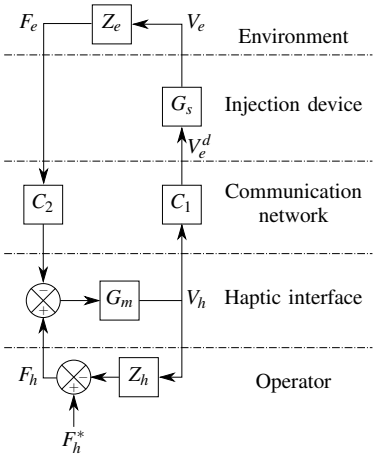

Figure 9. Two-channel force-position teleoperation architecture.

Though a force-position architecture could be selected, the very slow cement injection speed makes it much preferable not to use the haptic interface position to drive the injection device but to prefer rate control strategy. In this case, the injection device velocity should correspond to the haptic interface position, i.e. $X_h \equiv V_e^d$ [25], which involves $C_1 = C_2^{-1} = \frac{\varepsilon}{s}$ where ε is a positive scale factor. This non-causal control requires filtering: $C_2 = C_1^{-1} = \frac{\lambda s}{\varepsilon(s+\lambda)}$, where λ is the cut-off frequency selected to limit the amplification of the noisy environment force signal.

B. Viscosity management

The bone cement viscosity management uses the thermal exchanger, the control of which goes far beyond the scope of the present article. Details can be found in previous publications by coauthors, whether for the modeling and identification of the cement viscosity evolution [26], [13] or for the closed-loop control [27]. However, for the present paper to be self contained, the main insights about viscosity management are summed up in the following.

Bone cement temperature results from the heat transfer between the copper and the flowing bone cement. A very ambitious objective would be to adopt a cascade regulation of viscosity with an inner loop for cement temperature control, and an outer loop to control viscosity. However, this seems out of reach at the moment as the whole system is very complex and highly nonlinear by several aspects: i) the TEMs are current-controlled and the Joule effect is a function that varies with the square of this current input; ii) it is difficult, nor impossible in a credible setup, to directly measure the flowing bone cement temperature at the system outlet in order to implement a feedback control, at least because sterility issues prohibit the use of temperature sensors in contact with the biomaterial; iii) the polymerization reaction is irreversible.

Therefore, the proposed solution consists in an all or nothing viscosity control with an inner temperature closed-loop control (see Figure 10). Since only measurements of the copper temperature T_{Cu} of the thermal exchanger are available, the cement temperature control results from the regulation of T_{Cu} combined with the numerical resolution of the continuous heat equation. Then, the cement viscosity is numerically estimated as explained hereafter. The closed-loop control of T_{Cu} can be more or less sophisticated, but as emphasized in [27], a simple Proportional-Integral-Derivative (PID) controller C_T, or a combination of two PID, one for cooling, one for heating, already offer very good results. The all or noting strategy implemented in controller C_η is also quite simple: the temperature reference is chosen in order to heat the cement if reference viscosity is not reached, and to cool it otherwise.

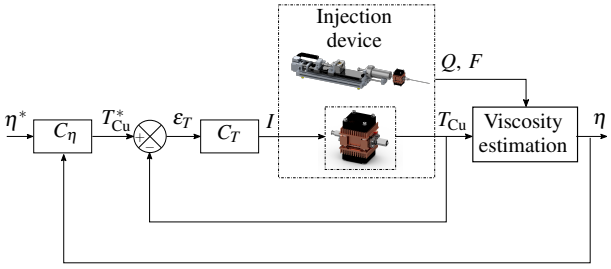

Figure 10. Viscosity/temperature control.

The previous strategy for the control of the cement polymerization not only relies on the ability to control the cement temperature, but also on the ability to estimate online the cement viscosity. It is based on the power-law (2), as in [5]. As assumed, during the design of the injection device, the flow involved in the injection is assimilated to a Poiseuille flow. Based on the assumption that the bone cement behavior can be described by the power-law, the principle of mass conservation coupled to the resolution of the Navier-Stokes equation provide the following relationship between the pressure drop ΔP and the flow rate Q:

$$Q = \left(\frac{\Delta P}{L_c}\right)^{\frac{1}{n}} \left(\frac{R_c}{2K}\right)^{\frac{1}{n}} \left(\frac{\pi n R_c^3}{3n+1}\right) \tag{3}$$

The detailed computation of this relation is given in Appendix. In order to compute online the bone cement viscosity, an adapted instrumentation has been included to the injection device as explained in section III-B2. The force sensor in the transmission provides the measurement of the injection force F, which in turn allows assessing the pressure drop:

$$\Delta P = \frac{F}{\pi R_s^2} - P_{\text{atm}} \tag{4}$$

with P_{atm} the atmospheric pressure. This implies two assumptions, which were verified using simulations or experimentally. On one side, the pressure at the outlet of the syringe is considered equal to the pressure on the plunger. On the other

side, the pressure at the outlet is supposed to be equal to the atmospheric pressure, i.e. it is assumed that the influence of the pressure within the vertebra is limited.

The carriage position measurement allows deriving the bone cement flow rate Q_v. Based on a rheological characterization [13], the flow index n is supposed to be constant over time and equal to 0.2. Thus, coupling equations 3 and 4 leads to express K at each time step. Finally, to reconstruct the viscosity value based on the power-law, the shear rate must be computed. According to calculations carried out in Appendix, the cement shear rate at a distance r from the flow centerline is:

$$\dot{\gamma} = \left(\frac{\Delta P}{2KL_c}\right)^{\frac{1}{n}} r^{\frac{1}{n}} \ . \tag{5}$$

With equation (3), it can be written as:

$$\dot{\gamma} = \frac{(3n+1)Q}{\pi n R_c^3}\left(\frac{r}{R_c}\right)^{\frac{1}{n}} \ . \tag{6}$$

The power-law is only valid above a certain shear rate (about 0.1 Pa·s). To ensure this validity at any non-zero velocity, the highest shear rate is considered, *i.e.* at $r = R_c$, which leads to compute the shear rate at the wall as:

$$\dot{\gamma}_{wall} = \frac{(3n+1)Q}{\pi n R_c^3} \ . \tag{7}$$

The online computation of the cement viscosity is then obtained from the power-law (2), with parameters n and K defined previously and $\dot{\gamma}$ computed from equation (7).

V. Experiments

A. Setup and measurements

Different experiments were carried out with the prototype at the Institute of Anatomy of the University Hospitals of Strasbourg. The cement was injected inside the lumbar and thoracic vertebrae of cadavers[2] for testings in conditions similar to usual practice, with the guidance of a fluoroscopy device (see Figure 11). In each of these experiments, bone cement Osteopal V® from Heraeus was prepared using conventional manual procedure and injected by experienced radiologists who use this cement in daily practice for more than 800 vertebral levels per year. It has to be mentioned that experiments on cadavers allow observing the effect of cement injection in bones which are no longer dense. However, this does not allow observing the effects of blood irrigation and of body temperature. Pre-clinical trials in animals were not performed as they were not justified: very dense vertebral bone would have been involved, which does not correspond to the case of patients suffering from VCF.

B. Assessment of the force feedback teleoperation strategy

The teleoperation strategy presented in section IV-A was implemented with the following gain adjustments for the rate control scheme: $\varepsilon = 0.91\text{mm}\cdot\text{s}^{-1}$ and $\lambda = 50\,\text{s}^{-1}$. At low

[2]The experiments on human specimens came were approved by the Department of Anatomy. All anatomical specimens used for this study were from human cadaver donations to this Department.

(a)

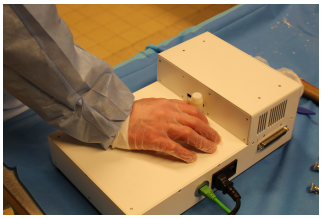

(b)

Figure 11. Operator during telemanipulation, at 2 m from the X-rays source: (a) operation field overview; (b) haptic interface operated by the radiologist.

injection velocities, effects of the quantization can be observed in the injection device velocity signal, since its resolution is $0.012\,\text{mm}\cdot\text{s}^{-1}$ while the average velocity is $0.141\,\text{mm}\cdot\text{s}^{-1}$ during the experiment. This has, however, no effect on the teleoperation performance, since the injection device velocity signal is not used in the teleoperation control. Plots in Figure 12 present typical data collected during an injection. They highlight several characteristics of vertebroplasty procedures, as well as characteristics of rate control teleoperation.

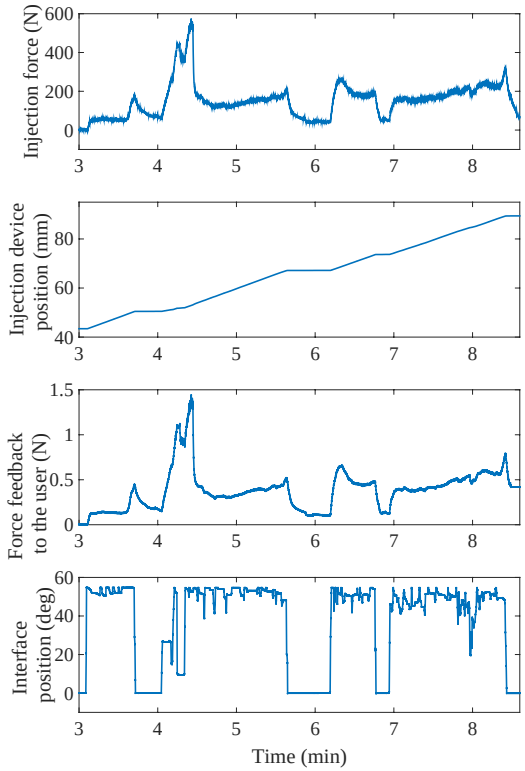

Figure 12. Force feedback teleoperation during injections into a vertebra.

First, it can be observed that the injection is performed in several phases, which allows checking how the cement spreads to prevent any leakage. During these imaging control phases, the interface is at the 0 deg position. The injection device is then motionless, and the cement injection is stopped. This particular injection was probably performed with less imaging control, and then pauses, than generally done. The operator preferred to limit doses as the imaging machine used at the Anatomy Department is of an old generation, and it tends to emit higher doses of X-rays. During the operation, it can be

observed that the forces at both the local and remote sites correspond to each other, with a scaling factor that makes force feedback range convenient for the operator. It can also be understood, though not directly observable, that the injection device position results from the integration of the haptic device position, according to the rate control principle. In this injection, it can also be observed that some peaks occur in the force signal, resulting from forming plugs in the injection conduit (visible at $t = 4.4$ min in the measured force), which is a well known issue in vertebroplasty, already discussed previously. Given the high power and control allowed by the robotic device, the radiologist could however perform the whole injection, such plugs being pushed efficiently.

Note : in addition to the assessment of the good operation of the bilateral teleoperation system in realistic intervention conditions, the system transparency was assessed in laboratory conditions, to check how the user experienced impedance Z_{th} compares to the environment impedance Z_e. The results, detailed in [23], show that impedance matching is very satisfactory with our teleoperation system, even for high viscosity values.

C. Assessment of the viscosity management

The strategy for the cement viscosity management is illustrated by the online computation of the estimated viscosity based on the bone cement viscosity model and on the system measurements of position and force, during a cement injection in another vertebra of the same cadaver. Figure 13 plots the online-computed viscosity, as described in section II-B4, together with the position of the injection device and the injection force. To obtain a satisfactory viscosity estimation,

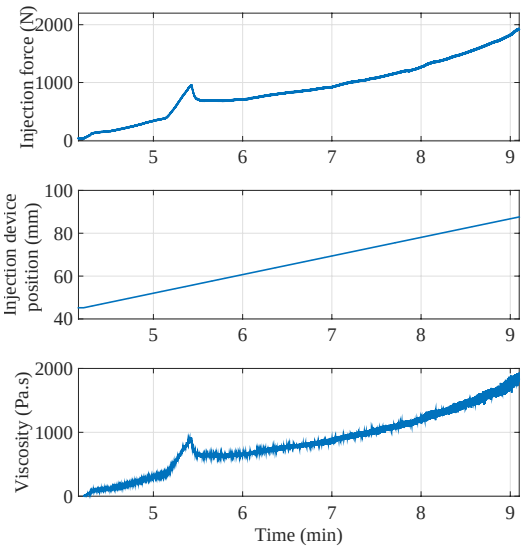

Figure 13. Online viscosity estimation with, from top to bottom, the injection force, the piston position and the reconstructed bone cement viscosity.

the cement is injected after conventional rest following the mixture. An additional resting phase is applied to let the cement harden. The injection then starts and is continuous and very slow during the rest of the experiment. The viscosity estimation allows having information about the cement state, and forecast the cement evolution. In this injection, it can be observed that the cement viscosity remains perfectly compatible with the limit values specified to limit cement leakages and to allow an easy injection. The presence of a small plug during the injection is clearly visible between $t = 5.15$ min and $t = 5.5$ min. As the model used to estimate viscosity cannot take such phenomenon into account, the viscosity estimation is then no longer accurate, which is clearly visible as the cement viscosity cannot decrease. After this transient, the viscosity estimation recovers to normal operation.

Finally, it is important to note that a manual system such as the Optimed Cemento MP® [19] would have been broken at the pressures required to perform the whole injection (at the syringe level, in spite of reinforcements of the glass syringe).

D. Assessment of the X-rays protection

During some injections, the practitioner wore a dosimeter while another one was placed on the injection device and a last one on the injection device. The haptic interface handle is only a few (2 to 3) meters away from the cadaver, whereas the injection device is in the fluoroscope zone, receiving a maximum of radiation doses. Plots presented in Figure 14 correspond to complete procedures, from the needles placements in the vertebral body to the bone cement injection. More precisely, four teleoperated injections with the presented system and one with a manual Optimed Cemento MP® device were performed. It can be noticed that the cumulative dose is in a ratio of 1 to 21 between measurements made on the user interface and on the injection device, respectively. It can also be observed that the radiologist dose was already severely increased by performing only one manual injection. In conclusion, the operator zone can be considered as safe.

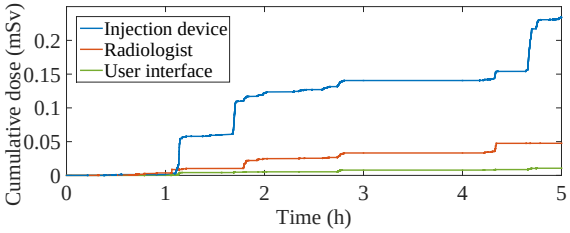

Figure 14. Cumulative dose over an experimental day.

VI. Conclusion

This article has presented the design and evaluation of a system dedicated to bone cement injection. Based on specifications resulting from the analysis of vertebroplasty procedures, the selected solution consists in a teleoperation device with force feedback, operated in rate-control in order to allow very slow injections. It improves radiologist practice, allowing advanced control over the injection, which can be performed at a distance to protect from X-rays, at high pressures, and with appropriate information feedback. Advanced viscosity supervision is made available, based on thermal regulation of the cement temperature both in the syringe and the injection pipe. This novel design was made possible by the fine analysis

of the medical practice, of the cement injection process, both in laboratory and realistic experimental conditions.

Perspectives of this work are related to the system development towards its clinical use. A first solution would be to apply the proposed principles to design a completely passive device, thus limiting safety issues, at the expense of some functionalities. A second solution, more ambitious, would consist in developing further the system safety features. This includes to design another thermal exchanger with active parts away from the patient, or to ensure bilateral teleoperation stability over the range of considered viscosity values. Finally, the most difficult challenge would be to consider viscosity feedback control not based on an all or nothing strategy but on an advanced control technique using the prediction of the cement viscosity in an optimal way.

ACKNOWLEDGMENT

Many thanks go to F. Schmitt for the mechanical design of the system. This longtime work benefited from many interdisciplinary interactions with colleagues, I. Bara for control, P. Rao for interventional radiology, and former MSc. students E. Sallord and R. Porto. We express our gratitude to Heraeus Medical for their donations, and to SATT Conectus and the French program Investissements d'Avenir Robotex and Labex CAMI (ANR-10-EQPX-44 and ANR-11-LABX-0004) for their financial support.

APPENDIX

Flow of a power-law fluid in a straight circular tube

Similar to a capillary rheometer, our injection device is designed such that a piston generates pressure on the bone cement inside the syringe (acting as reservoir) in order to force the cement to flow with a particular speed distribution across a capillary tube of length L and of radius R with $L >> R$ as illustrated in figure 15. Assumptions about the

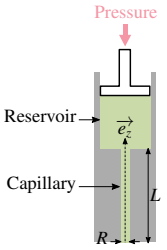

Figure 15. Geometry of the PMMA flow.

flow inside the capillary are similar to the classical Poiseuille model: i) the flow is isothermal, axisymmetric, stationary and incompressible; ii) the no-slip boundary condition is valid, which means that the velocity at the wall is zero; iii) a pressure gradient is generated in the longitudinal axis $\vec{e_z}$, which implies liquid layers sliding over each other and thus, velocity, are parallel to $\vec{e_z}$; iv) the pressure gradient is assumed to be negative when the flow is in the direction of positive z.

In our context, the symmetric strain rate tensor is written:

$$\left[\overline{\overline{\mathbf{D}}}\right] = \begin{pmatrix} 0 & 0 & \frac{1}{2}\frac{\partial V_z}{\partial r} \\ 0 & 0 & 0 \\ \frac{1}{2}\frac{\partial V_z}{\partial r} & 0 & \frac{\partial V_z}{\partial z} \end{pmatrix}_{(\vec{e}_r, \vec{e}_\theta, \vec{e}_z)} . \tag{8}$$

For a generalized Newtonian flow, the relation between the strain rate tensor and the Cauchy stress tensor is expressed as:

$$\overline{\overline{\boldsymbol{\sigma}}} = -p\bar{\bar{\mathbf{I}}} + 2\eta(\dot{\gamma})\overline{\overline{\mathbf{D}}} + \left(\kappa - \frac{2}{3}\eta\right)\vec{\nabla}.\vec{V}\bar{\bar{\mathbf{I}}} \tag{9}$$

where p is the thermodynamic pressure, $\bar{\bar{\mathbf{I}}}$ represents the second-order identity tensor, η denotes the dynamic viscosity and κ the bulk viscosity, $\dot{\gamma} = \sqrt{2II_{\mathbf{D}}}$ is the magnitude of the strain rate tensor, and $II_{\mathbf{D}}$ is the second invariant of $\overline{\overline{\mathbf{D}}}$.

In fluid dynamics, the principle of mass conservation applied to an incompressible fluid states that $\rho\vec{\nabla}\cdot\vec{V} = 0$. It results that equation (9) simplifies into:

$$\overline{\overline{\boldsymbol{\sigma}}} = -p\bar{\bar{\mathbf{I}}} + 2\eta(\dot{\gamma})\overline{\overline{\mathbf{D}}} \quad \text{and} \quad V_z \equiv V_z(r) \tag{10}$$

From equation (10) the stress tensor can be expressed in the coordinate reference $(\vec{e_r}, \vec{e_\theta}, \vec{e_z})$ as:

$$\left[\overline{\overline{\boldsymbol{\sigma}}}\right] = \begin{pmatrix} -p & 0 & \eta\frac{\partial V_z}{\partial r} \\ 0 & -p & 0 \\ \eta\frac{\partial V_z}{\partial r} & 0 & -p \end{pmatrix}_{(\vec{e_r}, \vec{e_\theta}, \vec{e_z})} . \tag{11}$$

The general Navier-Stokes equation yields:

$$\rho\frac{D\vec{V}}{Dt} = \vec{\nabla}\cdot\overline{\overline{\boldsymbol{\sigma}}} + \rho\vec{g} \tag{12}$$

with $\frac{D\vec{V}}{Dt} = \frac{\partial\vec{V}}{\partial t} + (\vec{V}\cdot\vec{\nabla})\vec{V}$, the material derivative of the velocity vector field, and $\vec{g}$, the gravitational field. Gravity is assumed to be negligible. Then, given the stationary assumption and the fact that the inertia term is zero, the movement equation becomes:

$$\vec{0} = \vec{\nabla}\cdot\overline{\overline{\boldsymbol{\sigma}}}' - \vec{\nabla}p \tag{13}$$

where $\overline{\overline{\sigma'}} = 2\eta(\dot{\gamma})\overline{\overline{\mathbf{D}}}$. Therefore, the cylindrical projection of equation (13) allows writing:

$$-\frac{\partial p}{\partial z} + \frac{1}{r}\frac{\partial r\sigma'_{rz}}{\partial r} = 0 \tag{14}$$

From equation (14), using the separation of variables, it comes first that:

$$\frac{\partial p}{\partial z} = -\frac{\Delta P}{L} \tag{15}$$

with $\Delta P = P_{\text{inlet}} - P_{\text{outlet}} > 0$, the pressure drop along the capillary of length L. Moreover, with the zero shear stress on the symmetry axis[3], the integration of (14) gives:

$$\sigma'_{rz}(r) = -\frac{\Delta P}{L}\frac{r}{2}. \tag{16}$$

The previous relation is valid no matter the viscosity law. In the following the previous computations are applied to bone

[3]On the symmetry axis the derivative of the velocity is null, and thus, the shear stress is also null.

cement, characterized by the non-Newtonian power-law (2) viscosity. According to equation (11) and since the velocity is decreasing, it can be written:

$$\sigma_{rz}^{'} = \eta(\dot{\gamma})\frac{\partial V_z(r)}{\partial r} \quad \text{with} \quad \dot{\gamma} = -\frac{\partial V_z(r)}{\partial r}. \tag{17}$$

From the power-law model (2) and the equation (17), $\sigma_{rz}^{'}$ is equivalent to:

$$\sigma_{rz}^{'} = -K\left(-\frac{\partial V_z(r)}{\partial r}\right)^n. \tag{18}$$

Taking into account the no-slip boundary condition, $V_z(r)$ can then be computed from equation (16):

$$V_z(r) = \frac{n}{n+1}\left(\frac{\Delta P}{2KL}\right)^{\frac{1}{n}}\left(R^{\frac{n+1}{n}} - r^{\frac{n+1}{n}}\right). \tag{19}$$

Finally, the flow rate Q and shear rate at the wall $\dot{\gamma}_{wall}$ are:

$$Q = \left(\frac{\Delta P}{L}\right)^{\frac{1}{n}}\left(\frac{R}{2K}\right)^{\frac{1}{n}}\left(\frac{\pi n R^3}{3n+1}\right) \tag{20}$$

$$\dot{\gamma}_{wall} = \frac{Q}{\pi R^3}\frac{3n+1}{n}. \tag{21}$$

REFERENCES

[1] J. A. Kanis *et al.*, "European guidance for the diagnosis and management of osteoporosis in postmenopausal women," *Osteoporosis International*, vol. 24, no. 1, pp. 23–57, 2013.

[2] C. A. H. Klazen *et al.*, "Vertebroplasty Versus Conservative Treatment in Acute Osteoporotic Vertebral Compression Fractures (Vertos II): an Open-Label Randomised Trial," *The Lancet*, vol. 376, no. 9746, pp. 1085–1092, 2010.

[3] J. C. Eck *et al.*, "Comparison of vertebroplasty and balloon kyphoplasty for treatment of vertebral compression fractures: a meta-analysis of the literature," *The Spine Journal*, vol. 8, no. 3, pp. 488–497, 2008.

[4] R. Schmidt *et al.*, "Cement leakage during vertebroplasty: an underestimated problem?" *European Spine Journal*, vol. 14, no. 5, pp. 466–473, 2005.

[5] M. Loeffel *et al.*, "Development of a computer-assisted high-pressure injection device for vertebroplasty," *IEEE Transactions on Biomedical Engineering*, vol. 54, no. 11, pp. 2051–2056, 2007.

[6] Merit Medical, "Stabilit® vertebral augmentation system," 2020. [Online]. Available: https://www.merit.com/merit-interventional/vertebral-compression-fracture/

[7] A. Gangi, B. A. Kastler, and J.-L. Dietemann, "Percutaneous vertebroplasty guided by a combination of ct and fluoroscopy," *American Journal of Neuroradiology*, vol. 15, no. 1, pp. 83–86, 1994.

[8] I. G. Hide and A. Gangi, "Percutaneous vertebroplasty: history, technique and current perspectives," *Clinical Radiology*, vol. 59, no. 6, pp. 461–467, 2004.

[9] A. Gangi *et al.*, "Quality assurance guidelines for percutaneous vertebroplasty," *Cardiovascular and Interventional Radiology*, vol. 29, no. 2, pp. 173–178, 2006.

[10] A. Komemushi *et al.*, "Radiation exposure to operators during vertebroplasty." *Journal of Vascular and Interventional Radiology*, vol. 16, no. 10, pp. 1327–32, 2005.

[11] G. Baroud, "Bone cement delivery system," International Patent US 20 130 123 790 A1, 2013.

[12] D. Giannitsios *et al.*, "High cement viscosity reduces leakage risk in vertebroplasty," in *5th Combined Meeting of the Orthopaedic Research Societies of Canada, USA, Japan and Europe*, 2004, p. 54.

[13] N. Lepoutre *et al.*, "Bone Cement Modeling for Percutaneous Vertebroplasty," *Journal of Biomedical Materials Research Part B: Applied Biomaterials*, September 2018.

[14] S. J. L. Sullivan and L. D. T. Topoleski, "Influence of Initial Component Temperature on the Apparent Viscosity and Handling Characteristics of Acrylic (PMMA) Bone Cement," *Journal of Biomedical Materials Research Part B: Applied Biomaterials*, vol. 81B, no. 1, pp. 224–230, 2007.

[15] International Organization for Standardization, *ISO 5833:2002 Implants for surgery — Acrylic resin cements*, Std., May 2002.

[16] S. Kolmeder and A. Lion, "On the thermomechanical-chemically coupled behavior of acrylic bone cements: experimental characterization of material behavior and modeling approach," *Technische Mechanik*, vol. 30, no. 1-3, pp. 195–202, 2010.

[17] DePuy Synthes, "Vertebroplasty devices," 2020. [Online]. Available: https://www.depuysynthes.com/hcp/spine/products?fq=Vertebroplasty

[18] Stryker, "Precision cement delivery system," 2020. [Online]. Available: https://www.stryker.com/us/en/portfolios/medical-surgical-equipment/image-guided-therapies/vertebral-compression-fractures.html

[19] OptiMed, "Cemento-MP," 2020. [Online]. Available: https://www.optimed.com/nc/en/products/category/spine/p-kategorie/spine/

[20] M. Loeffel, I. P. Pappas, and L.-P. Nolte, "Injection device with haptic feedback," International Patent US 20 090 216 191 A1, 2009.

[21] Ardes, "10 mL reusable syringe," 2018. [Online]. Available: http://www.ardes-group.com/blog/produit/seringue-10cc/

[22] R. B. Bird, R. C. Amstrong, and O. Assager, *Dynamics of Polymeric Liquids, Volume 1: Fluid Mechanics*. A Wiley-Interscience Publication, John Wiley & Sons, 1987.

[23] N. Lepoutre *et al.*, "Robotically assisted injection of orthopedic cement: System design, control and modeling," in *European Control Conference (ECC)*, Aalborg, Denmark, 2016, pp. 2127–2132.

[24] K. Hashtrudi-Zaad and S. E. Salcudean, "Analysis of control architectures for teleoperation systems with impedance/admittance master and slave manipulators," *The International Journal of Robotics Research*, vol. 20, no. 6, pp. 419–445, 2001.

[25] F. Mobasser and K. Hashtrudi-Zaad, "Transparent rate mode bilateral teleoperation control," *The International Journal of Robotics Research*, vol. 27, no. 1, pp. 57–72, 2008.

[26] N. Lepoutre *et al.*, "Design and control of a thermal device for bone cement injection," in *IEEE International Conference on Biomedical Robotics and Biomechatronics (BioRob)*, Singapore, 2016, pp. 508–513.

[27] ——, "Phase Space Identification Method for Modeling the Viscosity of Bone Cement," in *European Control Conference (ECC)*, June 2016, pp. 2404–2409.